RESEARCH ARTICLE | FEBRUARY 12 2025

Giant persistent photoconductivity at room temperature in Sn-based perovskites

Julie Euvrard ; Sadaf Pournia ; Oki Gunawan ; David B. Mitzi

Appl. Phys. Lett. 126, 063302 (2025)
https://doi.org/10.1063/5.0246648
CHORUS

Applied Physics Letters ARTICLE pubs.aip.org/aip/apl

Giant persistent photoconductivity at room temperature in Sn-based perovskites

Cite as: Appl. Phys. Lett. **126**, 063302 (2025); doi: 10.1063/5.0246648
Submitted: 3 November 2024 · Accepted: 23 January 2025 ·
Published Online: 12 February 2025

View Online Export Citation CrossMark

Julie Euvrard,[1,a)] Sadaf Pournia,[2] Oki Gunawan,[3] and David B. Mitzi[2,4,a)]

AFFILIATIONS

[1]Department of Physics and Centre for Processable Electronics, Imperial College London, London SW7 2BW, United Kingdom
[2]Department of Mechanical Engineering and Materials Science, Duke University, Durham, North Carolina 27708, USA
[3]IBM T. J. Watson Research Center, Yorktown Heights, New York 10598, USA
[4]Department of Chemistry, Duke University, Durham, North Carolina 27708, USA

[a)]**Authors to whom correspondence should be addressed:** julie.euvrard@imperial.ac.uk and david.mitzi@duke.edu

ABSTRACT

Long avoided due to adverse effects in traditional optoelectronic devices, persistent photoconductivity (PPC) is now sought-after for emerging technologies, including artificial synapses and coupled solar batteries. We report on a giant PPC effect at room temperature in the mixed Sn/Pb-based perovskite $MAPb_{0.5}Sn_{0.5}I_3$ (MA = methylammonium). Using Hall and photo-Hall measurements, we identify macroscopic separation of negative and positive carriers as the most likely origin for delayed photoconductivity decay, with a strong electron localization expected at grain boundaries or cracks within the polycrystalline films. Additionally, measurements on perovskite films with varying morphology and SnF_2 additive content reveal that large apparent grain size (>5 μm) and effective passivation of recombination centers combine to provide a path for achieving PPC extending over 100 h at room temperature.

While persistent photoconductivity (PPC) is generally observed at low temperatures in some technologically important inorganic semiconductors, including GaN, AlGaAs, and a-Si:H,[1–4] large PPC has been reported at room temperature in amorphous oxide semiconductors and harvested for neuromorphic devices requiring light-induced memory behavior.[5,6] The PPC effect has also been reported in tin-based oxide perovskites, where photoconductivity persists for up to several hours and is attributed to oxygen vacancies that form deep-level defects.[7,8] In tin-based halide perovskites, a PPC has been measured, yet with a relatively short memory of ∼300 s without the use of heterostructures.[9,10] Underlying mechanisms leading to PPC remain unclear, and various trapping mechanisms, including dangling bonds and Sn vacancies, have been proposed to explain delayed charge release at various timescales. Technologies such as photo-charged coupled solar batteries and optoelectronic synapses for long-term plasticity require a substantial PPC effect extending over hours to days.[6,11–13] The potential of a mixed Sn/Pb-based perovskite to achieve photocurrent decays over 100 h (i.e., giant PPC) at room temperature is, therefore, explored in this study. Hall effect measurements are performed to differentiate the contribution of carrier density and mobility to the PPC. Detailed study of carrier density decay enables the identification of an underlying mechanism of PPC in Sn-based perovskites. We further explore the impact of initial photocarrier density, and therefore charge recombination, to the extent of PPC. Finally, we perform measurements on perovskite samples with varying apparent grain sizes to uncover a process enabling spatial separation of carriers.

$MAPb_{0.5}Sn_{0.5}I_3$ (MA: methylammonium) samples with gold electrodes were prepared by solution processing for Hall effect measurements. Details on the film and device fabrication are provided in the supplementary material. Variations in apparent grain sizes are obtained by tuning the crystallization rate through antisolvent use (or not). SnF_2 addition has been employed and varied to control defect formation and prevent Sn^{2+} oxidation, stabilizing Sn-based perovskite devices for measurements.[14–16] X-ray diffraction (XRD) and scanning electron microscopy (SEM) were performed to monitor the film quality and morphology. Hall and photo-Hall effects were carried out using a parallel dipole line system that generates single harmonic oscillating magnetic field and using lock-in detection.[17] Lasers with above bandgap wavelengths were used to illuminate the samples, and the light intensity was tuned with neutral density filters. Equipment and experimental techniques are detailed in the supplementary material.

Figure 1(a) displays the time evolution of the conductivity σ, the positive Hall density corresponding to holes p_{Hall}, and the Hall mobility μ_{Hall}, for an exemplary $MAPb_{0.5}Sn_{0.5}I_3$ film prepared using 5% SnF_2 and no antisolvent during spin coating. The corresponding SEM image and XRD of this sample appear in the supplementary material (Fig. S2). The samples are measured for 1 h in the dark prior to illumination, for 1.5 h under illumination, and for 103 h in the dark after illumination. We observe a slow rise in conductivity under illumination, and an even slower conductivity decrease in the dark without reaching the dark background level within 100 h. A final dark conductivity lower than the pre-illumination dark conductivity points to a history-related effect for the sample response. Prior to the PPC measurement, the sample was left in the dark for ~12 h, while over 100 h are necessary to reach steady-state in the dark.

Using Hall effect measurements, we dissociate the contribution of carrier density and mobility to the PPC. While the time evolution of μ_{Hall} remains within the same order of magnitude, p_{Hall} decreases by two orders of magnitude over ~100 h in the dark, following a similar behavior to conductivity. The Hall coefficient remains positive throughout the experiment, suggesting that holes remain the primary charge carrier type under illumination and in the dark. This observation agrees with the known p-type character of mixed lead-tin perovskite through oxidation of Sn^{2+} (and associated defect formation).[18] The potential contribution of sample degradation or ionic motion through bias stress has been addressed through successive PPC measurements and incorporating large periods (minutes to hours) with no bias between measurements (Fig. S3). Notably, typically reported carrier densities for mixed Sn/Pb-based perovskites are several orders of magnitude higher than the value of $\sim 6 \times 10^{15}$ cm^{-3} obtained after a four-day decay in the current study.[14,19] In light of the severe PPC effect observed, it appears crucial to ensure sufficient time in the dark before performing conductivity measurements on such samples, to avoid the impact of residual photogenerated carriers. A slow decay in conductivity could be misinterpreted (given a short wait time) as a normal high background carrier density level.

To identify the underlying mechanism leading to the PPC effect, the time dependency of p_{Hall} in the dark is explored. PPC generally derives from an obstruction in carrier recombination and can be due to macroscopic barriers in space or microscopic barriers due to lattice relaxation.[13,20] Barriers in configurational space can be due to DX (donor) or AX (acceptor) centers with strong lattice relaxation.[2,21] Such barriers in configurational space can be difficult to differentiate from barriers in real space, which generally originate from inhomogeneities in doping or composition.[22,23] Heterostructures can also be engineered to enable macroscopic separation of charge carriers.[24,25] While stretched exponential decays associated with distributions of defects are widely used to fit and analyze PPC,[4,26–29] Queisser and Theodorou[2] suggest that a logarithmic decay should be attributed to the spatial separation of carriers. When inhomogeneous distributions of positive and negative carriers arise, the decay appears fast toward the beginning as carriers close to the boundaries recombine quickly and slow down as carriers further away reach the boundaries. This recombination kinetics can be monitored by probing the evolution of free carriers over time by the Hall effect. In Fig. 1(b), we observe a linear fit of the p_{Hall} decay when plotted in x-log y-lin configuration, suggesting a logarithmic photocurrent decay over a relatively long period of the study. Exponential and power law decays are, however, less probable as more significant deviations from a linear fit are observed when plotted in x-log y-log or x-lin y-log configurations. We, therefore, identify macroscopic barriers with spatial separation of carriers as the most likely origin of PPC in $MAPb_{0.5}Sn_{0.5}I_3$.

A possible source for the formation of inhomogeneous regions may relate to the use of the SnF_2 additive in the fabrication of $MAPb_{0.5}Sn_{0.5}I_3$ films (5% in the sample presented in Fig. 1). To

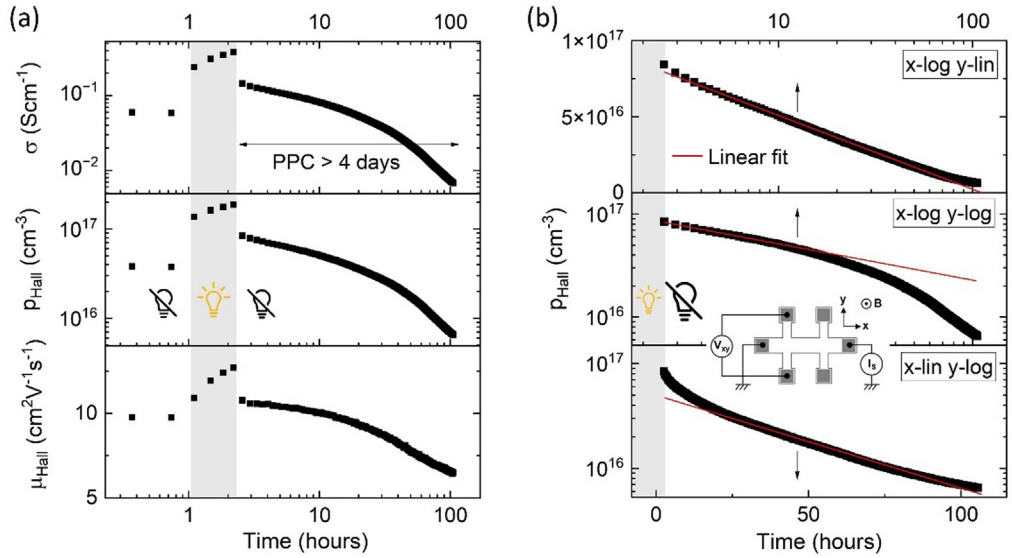

FIG. 1. (a) Conductivity (σ), Hall density (p_{Hall}), and Hall mobility (μ_{Hall}) before, under, and after illumination (638 nm; 30 mW/cm^2) over >100 h in total. The regions identified with the black and yellow lightbulbs correspond to dark and light conditions, respectively. (b) Hall density with respect to time plotted in x-log y-lin, x-log y-log, and x-lin y-log configurations. The red line corresponds to the linear fit for each plotting approach. The inset in (b) displays a schematic of transverse V_{xy} voltage extraction upon application of a current source I_S and magnetic field B on a Hall bar. Samples were left for 12 h in the dark prior to initial measurements.

explore this possibility, Fig. 2(a) displays the time evolution of p_{Hall} in $MAPb_{0.5}Sn_{0.5}I_3$ samples with varying SnF_2 concentrations of 0%, 5%, 10%, and 20% (in molar ratio relative to the combined Sn/Pb metal content). Apparent grain sizes from SEM images (likely reflecting cracking and other film formation features associated with solvent evaporation as well as nucleation/growth of grains) are maintained in a similar range (~2–5 μm) among all four concentrations (Fig. S4). XRD and EDS analyses suggest that crystallites forming at grain boundaries upon SnF_2 addition in the precursor solution are primarily associated with a SnI_2 phase (Figs. S5 and S6).

While initial inspection of Fig. 2 seems to suggest that PPC becomes more severe (longer decay time) with increasing SnF_2 concentration, a drastic increase in photocarrier density is also observed under illumination for such conditions, consistent with the increase in charge carrier recombination lifetime generally observed with extra SnF_2 in tin-based perovskites.[15,30] The starting density p_0 when light is turned off varies over two orders of magnitude from 0% to 20% SnF_2. For macroscopic separation of charges, the temporal decay of the carrier density depends on the profile of the charges built up in separate regions. Considering rectangular profiles, the evolution of $p(t)/p_0$ follows the analytical expression:[2]

$$\frac{p(t)}{p_0} = 1 - \frac{A}{p_0}\ln\left(1 + \frac{t}{\tau_0}\right), \tag{1}$$

where τ_0 is the lifetime for vanishing spatial separation and A reflects charge carrier recombination during the initial decay time τ_0. For time scales larger than τ_0 ($t \gg \tau_0$), Eq. (1) can be simplified to

$$\frac{p(t)}{p_0} = 1 - \frac{A}{p_0}\ln\left(\frac{t}{\tau_0}\right). \tag{2}$$

Figure 2(b) displays the fit of $p(t)/p_0$ for various SnF_2 concentrations to Eq. (2). Deviations from a simple logarithmic decay can be expected at long time scales due to inaccuracies in the carrier profile considered (i.e., not a perfectly rectangular profile). As a similar slope is obtained for all SnF_2 concentrations, we conclude that SnF_2 does not directly account for the PPC effect. Instead, SnF_2 likely passivates defects in $MAPb_{0.5}Sn_{0.5}I_3$, leading to an increase in photocarrier density upon illumination. We further explore this hypothesis by measuring the decay after illumination for two light intensities and two different wavelengths (above bandgap) with varying absorption coefficients for the 20% SnF_2 film (Fig. S7), which exhibit similar decay trends.

While the SnF_2 additive does not directly cause the PPC effect, we do observe a possible correlation between apparent grain size assessed from cracks in SEM images and the extent of the photocurrent decay. For a SnF_2 concentration of 5%, a stronger PPC effect over 100 h is measured for an average apparent grain size of 9 ± 5 μm (sample displayed in Figs. 1 and S2), while a smaller apparent grain size of 5 ± 3 μm [sample displayed in Figs. 2 and S4(b)] provides an almost complete decay within 5–10 h. To assess the impact of the size of crystalline regions on PPC, additional $MAPb_{0.5}Sn_{0.5}I_3$ samples with varying morphology (controlled by film deposition; see Methods) and SnF_2 concentrations have been fabricated and measured (e.g., see Fig. S8). We note that no impact of SnF_2 concentration or morphology is observed on hole mobility extracted from Hall measurements (see Fig. S9). Figure 3(a) summarizes the ratio of charge carriers recombining within the time $e\tau_0$ after illumination stops (with e Euler's number), A/p_0, extracted from the fit of the decay with Eq. (2), as a function of apparent grain diameter D. The carrier density decay profiles for all additional samples are provided in the supplementary material (Fig. S10).

A/p_0 corresponds to the ratio of charge carriers recombining within $e\tau_0$ after the light is turned off and is, therefore, associated with a vanishing spatial separation. We can expect A/p_0 to depend on the extent of boundaries between electron- and hole-rich regions. We observe a clear correlation between the apparent grain size and the extracted parameters A/p_0 [Fig. 3(a)], while no correlation is observed with the SnF_2 concentration (Fig. S11). Most notably, we show the ratio of charge carriers initially recombining drops from ~25% to ~5% with increasing apparent grain size (smaller surface-to-volume ratio). It is, therefore, believed that the spatial separation of carriers

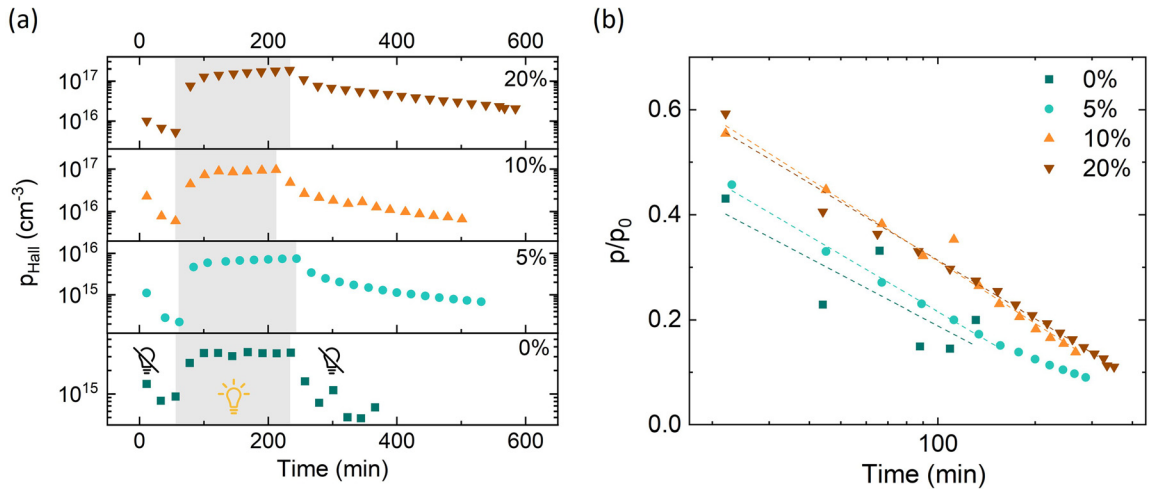

FIG. 2. (a) Time evolution of Hall density p_{Hall} before, under, and after illumination (520 nm; 1.2 mW/cm^2) for 0%, 5%, 10%, and 20% SnF_2. The regions identified with the black and yellow lightbulbs correspond to dark and light conditions, respectively. (b) Decay of the Hall density in the dark normalized to the density at $t = 0$, p_0, when the light is turned off. The dotted lines correspond to the linear fits in the x-log y-lin scale.

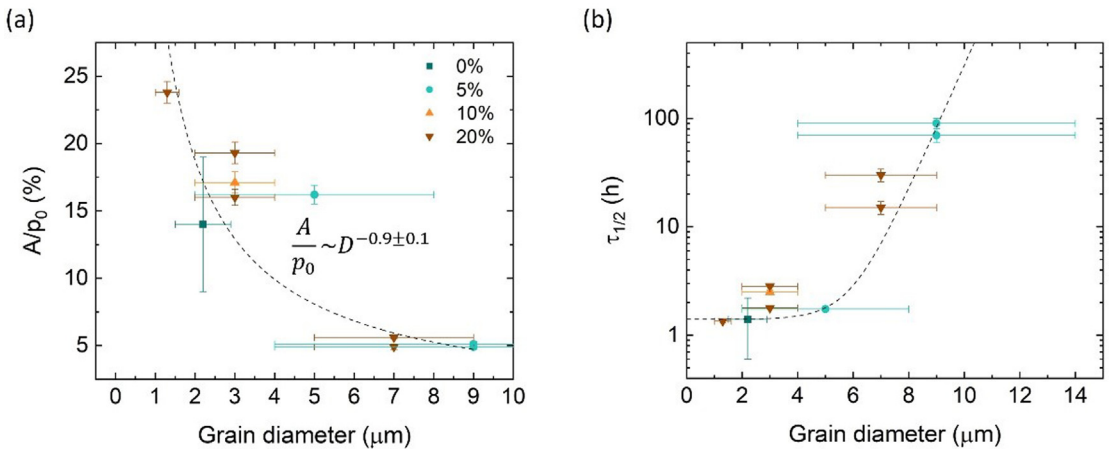

FIG. 3. Ratio of photogenerated carriers recombining within an initial decay time $e\tau_0$ (A/p_0) (a) and half lifetime $\tau_{1/2}$ (b) as a function of apparent grain diameter D. The legend showing percentages corresponds to SnF_2 concentrations. Data are obtained from a fit using Eq. (2). The dashed curve corresponds to a fit with a power law of D in (a), and to a guide to the eye based on an exponential behavior with D in (b).

may occur between grain boundaries or at cracks separating polycrystalline regions, as observed with SEM and grain interiors.

The expected evolution of A/p_0 with crystallite (grain or polycrystalline region separated by cracks) size can be modeled considering charge segregation between grain interior and boundaries of circular grains (Fig. S12). For simplicity, we consider that charge carriers at the grain boundaries are confined within a ring of negligible thickness l compared to the grain size. We can demonstrate (see the supplementary material for details) that the ratio A/p_0 is related to the grain diameter D according to

$$\frac{A}{p_0} \sim \frac{4l}{D}. \tag{3}$$

By fitting this function to our data, we find a good match with the inverse relation with D and extract a length l of 90 ± 20 nm. We, therefore, predict a negligible PPC for grain sizes ~ 200 nm or less. Note that an apparent grain size lying in the hundreds of nm range is generally reported for Sn-based films and devices,[31] suggesting that most studies may be impacted by only a mild PPC effect. However, depending on the measurement or application, the effect still could be significant. We also show an exponential dependence of the half lifetime $\tau_{1/2}$ with apparent grain size [Fig. 3(b)]. A similar behavior has been observed in doped superlattices with the modulation of band energies in alternating n-type, intrinsic, and p-type Si layers.[22] These results suggest that combining large grain size with high photocurrent through passivation may contribute to supporting a giant photoconductivity effect in $MAPb_{0.5}Sn_{0.5}I_3$.

We hypothesize that electron localization leads to PPC in $MAPb_{0.5}Sn_{0.5}I_3$. Using carrier-resolved photo-Hall (CRPH) technique, we have shown that the electron mobility is orders of magnitude smaller than the hole mobility $\mu_n \ll \mu_p$,[32] pointing to electrons being more prone to localization than holes in the $MAPb_{0.5}Sn_{0.5}I_3$ films. Charge localization through small polaron formation has been reported as favorable and recurrent in Sn-based perovskites according to density functional theory (DFT) calculations,[33–36] but investigations diverge regarding the nature of the localized charge (hole or electron). Additionally, DFT calculations suggest a higher stability for bipolaronic states compared to single-electron polarons.[33] A stabilization of single-electron polarons at defects expected at grain boundaries could facilitate bipolaron formation (Fig. 4).[33]

Considering electron traps at the grain boundaries, a downward band bending is expected.[37] Upon illumination, photogenerated electrons and holes are initially homogeneously distributed and recombine quickly. As electrons accumulate at grain boundaries, a built-in voltage between grain interior and grain boundary partially counteracts and reduces the initial band bending.[37] Net accumulation of electrons at the grain boundaries and holes in the grain interior slows down recombination, as reported for various polycrystalline materials, and can be used to engineer optoelectronic properties.[37] Self-localization of

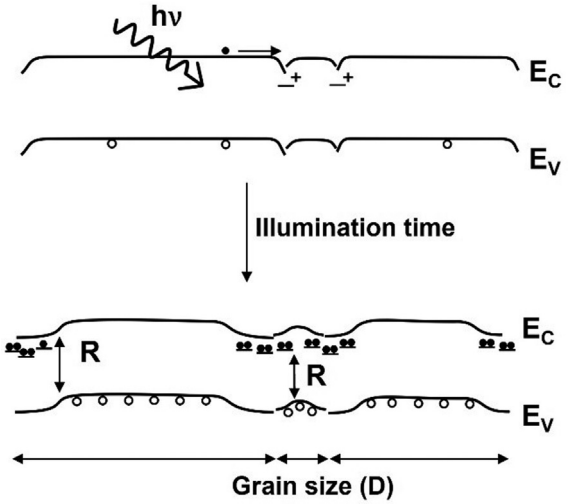

FIG. 4. Schematic view of a polycrystalline film band diagram with photocarrier generation as light is turned on (top) and after a long illumination time (bottom). Recombination (R) mainly occurs at the boundaries between the hole-rich and electron-rich regions. E_C and E_V correspond to conduction and valence band edges, respectively. $h\nu$ is used to label photons.

electrons, potentially stabilized through bipolaronic states formation, would progressively extend the electron-rich region toward the interior of the grain. As electrons and holes spatially separate, recombination slows down, and the photoconductivity increases. This progressive segregation of carriers explains the transient nature of the photocurrent rise under illumination. This model is also consistent with a steady-state regime being more quickly reached with decreasing light intensity as bipolaron formation becomes less likely (see Fig. S13). After illumination, closely-spaced pairs at the interface between the electron- and hole-rich regions recombine, leading to an initial fast photoconductivity decay. As more distant carriers diffuse toward the interface and recombine, a slower photoconductivity decay is observed. Therefore, films with larger grains (e.g., less cracks) exhibit a much stronger PPC effect than films with smaller grains. While a trapping/detrapping process closer to the microscopic barrier with lattice relaxation view is suggested in previous studies,[9,10] our analysis more strongly suggests a spatial separation of charges with the formation of macroscopic barriers. Interestingly, the extent of PPC is also observed to increase with the magnitude of the photocurrent reached in these studies, a behavior that would be consistent with our model.

In this study, we report a giant PPC at room temperature in mixed Sn/Pb-based halide perovskites. We hypothesize (and provide supporting data) that the PPC effect is most likely associated with the localization of electrons at defects at grain boundaries or cracks. The PPC effect can, therefore, be controlled by optimizing crystallite size and ensuring high photocurrent level through defect passivation, for example, with the use of SnF_2 additive. While PPC is detrimental for electronic applications requiring high switching speeds, such effect is of particular interest for neuromorphic applications.[6,12,38] Alternatively, increased charge carrier lifetime enabled by their spatial separation could be leveraged in solar cells, photocatalysis, and coupled solar batteries.[11,39]

See the supplementary material for details on the experimental methods.

This work was supported by the National Science Foundation under Grant No. 2004869.

AUTHOR DECLARATIONS

Conflict of Interest

D.B.M. was previously employed by and owns stock in IBM, the industrial partner in the NSF-GOALI project that sponsored this research.

Author Contributions

Julie Euvrard: Conceptualization (equal); Data curation (equal); Formal analysis (equal); Investigation (equal); Methodology (equal); Writing – original draft (equal); Writing – review & editing (equal). **Sadaf Pournia:** Data curation (equal); Formal analysis (supporting); Investigation (equal); Writing – original draft (supporting); Writing – review & editing (equal). **Oki Gunawan:** Investigation (supporting); Resources (equal); Writing – review & editing (equal). **David B. Mitzi:** Conceptualization (equal); Funding acquisition (equal); Resources (equal); Supervision (equal); Writing – review & editing (equal).

DATA AVAILABILITY

The data that support the findings of this study are available from the corresponding authors upon reasonable request.

REFERENCES

[1]H. M. Chen, Y. F. Chen, M. C. Lee, and M. S. Feng, "Persistent photoconductivity in *n*-type GaN," J. Appl. Phys. **82**(2), 899–901 (1997).
[2]H. J. Queisser and D. E. Theodorou, "Decay kinetics of persistent photoconductivity in semiconductors," Phys. Rev. B **33**(6), 4027–4033 (1986).
[3]R. J. Freitas and K. Shimakawa, "Kinetics of the persistent photocurrent in a-Si: H," Int. J. Mod. Phys. B **30**(14), 1650075 (2016).
[4]J. Y. Lin, A. Dissanayake, G. Brown, and H. X. Jiang, "Relaxation of persistent photoconductivity in $Al_{0.3}Ga_{0.7}As$," Phys. Rev. B **42**(9), 5855–5858 (1990).
[5]M. Lee, W. Lee, S. Choi, J. W. Jo, J. Kim, S. K. Park, and Y. H. Kim, "Brain-inspired photonic neuromorphic devices using photodynamic amorphous oxide semiconductors and their persistent photoconductivity," Adv. Mater. **29**(28), 1700951 (2017).
[6]S.-L. Gao, L.-P. Qiu, J. Zhang, W.-P. Han, S. Ramakrishna, and Y.-Z. Long, "Persistent photoconductivity of metal oxide semiconductors," ACS Appl. Electron. Mater. **6**(3), 1542–1561 (2024).
[7]J. Park, U. Kim, and K. Char, "Photoconductivity of transparent perovskite semiconductor $BaSnO_3$ and $SrTiO_3$ epitaxial thin films," Appl. Phys. Lett. **108**(9), 092106 (2016).
[8]Y. Lee, D. Yoon, S. Yu, H. Sim, Y. Park, Y. S. Nam, K. J. Kim, S. Y. Choi, Y. Kang, and J. Son, "Reversible manipulation of photoconductivity caused by surface oxygen vacancies in perovskite stannates with ultraviolet light," Adv. Mater. **34**(5), e2107650 (2022).
[9]C. K. Liu, Q. Tai, N. Wang, G. Tang, H. L. Loi, and F. Yan, "Sn-based perovskite for highly sensitive photodetectors," Adv. Sci. **6**(17), 1900751 (2019).
[10]Y. Sun, L. Qian, D. Xie, Y. Lin, M. Sun, W. Li, L. Ding, T. Ren, and T. Palacios, "Photoelectric synaptic plasticity realized by 2D perovskite," Adv. Funct. Mater. **29**(28), 1902538 (2019).
[11]Y.-X. Tan, X. Zhang, J. Lin, and Y. Wang, "A perspective on photoelectrochemical storage materials for coupled solar batteries," Energy Environ. Sci. **16**(6), 2432–2447 (2023).
[12]G. Vats, B. Hodges, A. J. Ferguson, L. M. Wheeler, and J. L. Blackburn, "Optical memory, switching, and neuromorphic functionality in metal halide perovskite materials and devices," Adv. Mater. **35**(37), e2205459 (2023).
[13]A. Sumanth, K. Lakshmi Ganapathi, M. S. Ramachandra Rao, and T. Dixit, "A review on realizing the modern optoelectronic applications through persistent photoconductivity," J. Phys. D **55**(39), 393001 (2022).
[14]Q. Chen, J. Luo, R. He, H. Lai, S. Ren, Y. Jiang, Z. Wan, W. Wang, X. Hao, Y. Wang *et al.*, "Unveiling roles of tin fluoride additives in high-efficiency low-bandgap mixed tin-lead perovskite solar cells," Adv. Energy Mater. **11**(29), 2101045 (2021).
[15]S. Gupta, D. Cahen, and G. Hodes, "How SnF_2 impacts the material properties of lead-free tin perovskites," J. Phys. Chem. C **122**(25), 13926–13936 (2018).
[16]J. Kurisinkal Pious, Y. Zwirner, H. Lai, S. Olthof, Q. Jeangros, E. Gilshtein, R. K. Kothandaraman, K. Artuk, P. Wechsler, C. Chen *et al.*, "Revealing the role of tin fluoride additive in narrow bandgap Pb-Sn perovskites for highly efficient flexible all-perovskite tandem cells," ACS Appl. Mater. Interfaces **15**(7), 10150–10157 (2023).
[17]O. Gunawan, Y. Virgus, and K. F. Tai, "A parallel dipole line system," Appl. Phys. Lett. **106**(6), 062407 (2015).
[18]Z. Zhang, Y. Huang, J. Jin, Y. Jiang, Y. Xu, J. Zhu, and D. Zhao, "Mechanistic understanding of oxidation of tin-based perovskite solar cells and mitigation strategies," Angew. Chem., Int. Ed. **62**(45), 202308093 (2023).
[19]K. J. Savill, A. M. Ulatowski, and L. M. Herz, "Optoelectronic properties of tin-lead halide perovskites," ACS Energy Lett. **6**(7), 2413–2426 (2021).
[20]H. J. Queisser, "Persistent photoconductivity in semiconductors," in *Proceedings of the 17th International Conference on the Physics of Semiconductors*, San Francisco, CA, August 6–10, 1985 (Springer, 1984), pp. 1303–1308.
[21]D. V. Lang and R. A. Logan, "Large-lattice-relaxation model for persistent photoconductivity in compound semiconductors," Phys. Rev. Lett. **39**(10), 635–639 (1977).

[22]M. Hundhausen, L. Ley, and R. Carius, "Carrier recombination times in amorphous-silicon doping superlattices," Phys. Rev. Lett. **53**(16), 1598–1601 (1984).
[23]H. X. Jiang and J. Y. Lin, "Persistent photoconductivity and related critical phenomena in $Zn_{0.3}Cd_{0.7}Se$," Phys. Rev. B **40**(14), 10025–10028 (1989).
[24]A. Tebano, E. Fabbri, D. Pergolesi, G. Balestrino, and E. Traversa, "Room-temperature giant persistent photoconductivity in $SrTiO_3/LaAlO_3$ heterostructures," ACS Nano **6**(2), 1278–1283 (2012).
[25]J. Hao, Y.-H. Kim, S. N. Habisreutinger, S. P. Harvey, E. M. Miller, S. M. Foradori, M. S. Arnold, Z. Song, Y. Yan, J. M. Luther *et al.*, "Low-energy room-temperature optical switching in mixed-dimensionality nanoscale perovskite heterojunctions," Sci. Adv. **7**, eabf1959 (2021).
[26]V. V. Ursaki, I. M. Tiginyanu, P. C. Ricci, A. Anedda, S. Hubbard, and D. Pavlidis, "Persistent photoconductivity and optical quenching of photocurrent in GaN layers under dual excitation," J. Appl. Phys. **94**(6), 3875–3882 (2003).
[27]H. Yin, A. Akey, and R. Jaramillo, "Large and persistent photoconductivity due to hole-hole correlation in CdS," Phys. Rev. Mater. **2**(8), 084602 (2018).
[28]H. X. Jiang and J. Y. Lin, "Percolation transition of persistent photoconductivity in II-VI mixed crystals," Phys. Rev. Lett. **64**(21), 2547–2550 (1990).
[29]R. J. Freitas and K. Shimakawa, "Persistent photocurrents and defects," in *Photoconductivity and Photoconductive Materials*, 1st ed. (John Wiley, 2022).
[30]K. J. Savill, A. M. Ulatowski, M. D. Farrar, M. B. Johnston, H. J. Snaith, and L. M. Herz, "Impact of tin fluoride additive on the properties of mixed tin-lead iodide perovskite semiconductors," Adv. Funct. Mater. **30**(52), 2005594 (2020).
[31]H. Dong, C. Ran, W. Gao, N. Sun, X. Liu, Y. Xia, Y. Chen, and W. Huang, "Crystallization dynamics of Sn-based perovskite thin films: Toward efficient and stable photovoltaic devices," Adv. Energy Mater. **12**(1), 2102213 (2022).
[32]J. Euvrard, O. Gunawan, X. Zhong, S. P. Harvey, A. Kahn, and D. B. Mitzi, "p-Type molecular doping by charge transfer in halide perovskite," Mater. Adv. **2**(9), 2956–2965 (2021).
[33]H. Ouhbi, F. Ambrosio, F. De Angelis, and J. Wiktor, "Strong electron localization in tin halide perovskites," J. Phys. Chem. Lett. **12**(22), 5339–5343 (2021).
[34]A. Mahata, D. Meggiolaro, and F. De Angelis, "From large to small polarons in lead, tin, and mixed lead-tin halide perovskites," J. Phys. Chem. Lett. **10**(8), 1790–1798 (2019).
[35]J. Yu, J. Kong, W. Hao, X. Guo, H. He, W. R. Leow, Z. Liu, P. Cai, G. Qian, S. Li *et al.*, "Broadband extrinsic self-trapped exciton emission in Sn-Doped 2D lead-halide perovskites," Adv. Mater. **31**(7), e1806385 (2019).
[36]T. Li, X. Chen, X. Wang, H. Lu, Y. Yan, M. C. Beard, and D. B. Mitzi, "Origin of broad-band emission and impact of structural dimensionality in tin-alloyed Ruddlesden–Popper hybrid lead iodide perovskites," ACS Energy Lett. **5**(2), 347–352 (2020).
[37]Z. Gao, C. Leng, H. Zhao, X. Wei, H. Shi, and Z. Xiao, "The electrical behaviors of grain boundaries in polycrystalline optoelectronic materials," Adv. Mater. **36**(4), e2304855 (2024).
[38]A. Mazumder, C. K. Nguyen, T. Aung, M. X. Low, M. A. Rahman, S. P. Russo, S. A. Tawfik, S. Wang, J. Bullock, V. Krishnamurthi *et al.*, "Long duration persistent photocurrent in 3 nm thin doped indium oxide for integrated light sensing and in-sensor neuromorphic computation," Adv. Funct. Mater. **33**(36), 2303641 (2023).
[39]J. Y. Y. Loh, G. Sharma, N. P. Kherani, and G. A. Ozin, "Post-illumination photoconductivity enables extension of photo-catalysis after sunset," Adv. Energy Mater. **11**(41), 2101566 (2021).